Multi-task Deep Neural Network for Intracardiac Activity Reconstruction in Atrial Fibrillation

Miriam Gutiérrez-Fernández[1], Miguel Ángel Cámara-Vázquez[1], Ismael Hernández-Romero[2], Carlos Fambuena-Santos[2], Maria S Guillem[2], Andreu M Climent[2], Karen López Linares[3,4], Óscar Barquero-Pérez[1]

[1] Universidad Rey Juan Carlos, Fuenlabrada, Madrid, Spain
[2] ITACA Institute, Universitat Politècnica de València, València, Spain
[3] Fundación Vicomtech, Basque Research and Technology Alliance (BRTA), Donostia, Spain
[4] eHealth group, Bioguipuzkoa Health Research Institute, Spain

Abstract

The reconstruction of cardiac mapping for arrhythmia characterization remains a challenge for both invasive and non-invasive approaches. This paper presents a novel data-driven approach using a multi-task deep neural network for the reconstruction of intracardiac activity from body surface potentials in atrial fibrillation patients. The proposed framework integrates 3D convolutions and Recurrent Neural Networks for spatio-temporal feature extraction from body surface potentials, enhancing the reconstruction of electrograms. Performance was evaluated against the Tikhonov method in synthetic and real data, showing robustness to noise and electrode disconnection.

1. Introduction

The management of patients with persistent atrial fibrillation (AF) remains a great cornerstone in the field of rhythm disorders. Although cardiac ablation is effective in many patients, there is still no clear consensus on the optimal ablation site [1]. Given this uncertainty, during invasive procedures electrophysiologists often perform pulmonary vein isolation (PVI), as the electrical maps reconstructed invasively during surgery do not yield enough spatial resolution to provide reliable decision-making support [2]. Yet, it has been demonstrated that there is no clear correlation between PVI and arrhythmia eradication, especially in the case of persistent AF where the success rate is roughly 40-60% [3].

Aware of this limitations, different methods have been proposed to improve cardiac mapping reconstructions from torso surface measurements on the perspective of improving atrial arrhythmia understanding and characterization. This is known as inverse problem; source potentials produced in the myocardium are attempted to be reconstructed from potentials measured on the torso. The inverse problem in electrocardiography is ill-posed due to the mathematical and physical nature of the problem. Electrocardiographic imaging (ECGI) consists in the reconstruction of intracardiac activity, i.e. electrograms (EGMs), body surface potentials (BSPs) and geometrical information from the patient's torso. Although this method provides overall good results, it involves using prior information apart from the BSPs to solve the inverse problem (the geometry of the patient's torso, usually provided by a Computed Tomography Scan), and it is sensitive to noise, hindering the robustness of the reconstructions [4].

Lately, research on novel methods based on artificial intelligence (AI) to overcome traditional ECGI limitations is being developed in similar clinical applications, where spatio-temporal data exploitation is key. The combination of signal-to-image transformations and computer vision algorithms can boost the ability to detect spatio-temporal correlations [5]. Specifically, many works have shown that the application of Deep Learning (DL) to the different stages of signal cardiac reconstruction is beneficial and can improve the current gold standard, namely Tikhonov Regularization, and other traditional optimization-based methods [6]. Specifically, when addressing the reconstruction of EGM from BSPs, the use of computer-vision architectures aims to disentangle the global conduction behaviour of the electrical wavefronts as they propagate across the torso, given that the apparent behaviour of BSPs in the temporal domain often seems unpredictable by their own [7–9].

In this work we propose a DL framework for intracardiac activity reconstruction in AF signals. This method leverages BSPs feature extraction for EGM reconstruction as a joint task. This is modelled as a 2-branch DL network combining 3D-convolutions (for spatio-temporal characterization) and Long Short-Term Memory (LSTM) layers (for temporal characterization). Robustness is measured

through realistic noise addition, multiple data layouts and electrode activation along the torso. Results are compared to Tikhonov reconstruction, the current gold standard.

2. Methods

This section presents the methodology used to develop and evaluate our approach.

2.1. Dataset of computerized models

EGMs were generated using one realistic computerized model of the atria (N=2039 nodes), with the atrial tissue represented by a simplified endocardium-epicardium layer, as previously done in [9, 10]. The forward problem is then computed to obtain the BSPs, using ten torso models (M=659 nodes). The resulting BSPs consist of 760 signals generated using different complexity propagation schemes and driver locations, sampled at $fs = 500\ Hz$ with a duration from 2 to 5 seconds [11]. Input BSPs are represented as 3D arrays, where the x and y dimensions correspond to the height and width of the image formed by the electrode information at each instant, and the z dimension corresponds to time. Here we work under the hypothesis that this rearrangement is beneficial for EGM reconstruction, as it is compatible with deep architectures that leverage knowledge contained not only between two consecutive time instants, but also between contiguous electrodes. Details on this transformation are explained in Section 2.2.2

2.2. Proposed approach

Spatio-temporal exploitation of BSPs is achieved using 2-branch network, each of them performing one task: a feature extraction network that processes the 3D images or arrays generated from BSP information, as explained in Sections 2.2.1 and 2.2.2, and a reconstruction network that aims to reproduce the original EGM. Figure 1 shows the general scheme of the proposed architecture, which is further described in Section 2.2.3. The former branch serves as a secondary task that enhances the main task, EGM reconstruction.

2.2.1. Pre-processing and temporal settings

First, the raw EGM signals are filtered using a Butterworth band-pass filter with a frequency range of 3 to 30 Hz. Next, when BSPs are computed, they are corrupted with white noise and electrode-movement noise (EM noise). The EM noise introduces additional uncertainty and approximates a real clinical setting. Real EM noise signals are extracted from the MIT-BIH Noise Stress Test Database [12]. EM noise is randomly applied to patches of 2x2 electrodes within the BSPs as shown in Figure 2. Then, the BSPs are filtered again using a 3-30 Hz Butterworth band-pass filter, which removes most artifacts originated noise sources. The signals are then down-sampled to a sampling frequency of 200 Hz to reduce temporal redundancy and facilitate training with smaller batches, which are better suited to the employed architectures. Finally, both EGMs and BSPs are normalized node-wise between -1 and 1 to ensure magnitude coherence throughout the network and to prevent vanishing or exploding gradients.

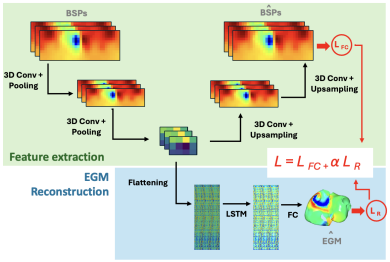

Figure 1. Architecture of the model. The loss function is weighted with the parameter α, assigning more weight to the main branch (EGM reconstruction).

2.2.2. Spatial processing of data

Aiming to exploit spatial and temporal information, BSPs are arranged in a rectangular array that follows the spatial layout on the torso, represented as $Nx6x16$ sets of images, where N is the number of temporal samples of each BSP signal. Linear interpolation is applied obtaining images of size $Nx16x32$. The final dataset consists of 76 EGM signals and 760 BSPs with 64 electrodes each, which is divided into training, testing, and validation subsets, comprising 80%, 15%, and 5% of the total models, respectively. To prevent information leakage from training to testing, the dataset is split EGM model-wise.

2.2.3. Architecture

Spatio-temporal feature extraction is accomplished using a 3D Convolutional Autoencoder (CAE) [13] commonly used for image analysis tasks. It has two main components: an encoder, which compresses the input data into a lower-dimensional representation known as the latent space, and a decoder branch, which reconstructs the original input from the latent space. By the use of convolutional layers the spatial local connectivity found in input images can be leveraged. The second branch aims to capture temporal correlations and maintain "memory" between frames by the use of LSTM layers.

The complete architecture is trained to minimize the following loss function L:

$$L = L_{FE} + \alpha\, L_R \tag{1}$$

where L_{FE} is the feature extraction loss computed as the RMSE between decoded BSPs and real BSPs, L_R is the

reconstruction loss computed as RMSE between reconstructed EGMs and real EGMs, and α is a weighted parameter fixed to a value of 2.5 to give more weight to the reconstruction loss during optimization. Regularization techniques such as dropout, early stopping, and L2 penalization are used during training to prevent overfitting.

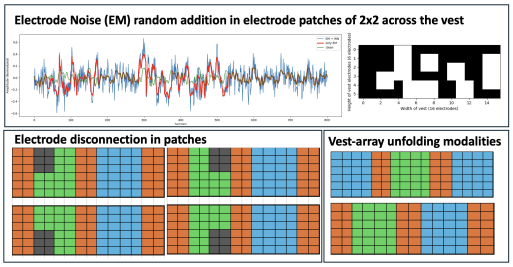

Figure 2. 1) Segments of real EM noise are randomly inserted into the space in patches, depicted as white squares. The green signal represents the original clean BSP, while the orange signal represents the addition of noise. The blue signal represents the final noisy signal, which includes both the added EM noise and white noise. 2) Four possible scenarios are replicated in E5-E8, where one patch of size 3x2 electrodes from the front side is disconnected in each experiment. In the figure, orange, green, and blue represent lateral (L), frontal (F), and back (B) electrodes, respectively. 3) Vest-Array unfolding modalities. When arranging the electrodes into a 2D array, two different arrangements are tested in E0 and E9. The top figure follows the order of F-L-B-L-F, while the bottom figure follows the order of L-B-L-B-L.

2.3. Performance metrics

To evaluate the performance of the model, the following well-known metrics are applied, which are used to assess two different signals depending on the network. In the CAE network, BSPs and reconstructed BSPs are evaluated using Root Mean Squared Error (RMSE) [14] and the Spearman Correlation Index (SCI) [15]. In the reconstruction network, the reconstructed EGMs are assessed using the original EGMs with the same metrics.

Furthermore, we compare the RMSE obtained using our method with the RMSE obtained when reconstructing the signal with the gold standard Zero-Order Tikhonov (ZOT) equation ([6]), which is computed as follows:

$$X = min\left[||AX - B||_2^2, +, \lambda^2||RX||_2^2\right] \quad (2)$$

where A is the transfer matrix, X is the EGM signals and R equals the identity matrix for ZOT, imposing a limit on the magnitude of the solution.

3. Results

The model's performance is evaluated on a test subset, using metrics from Section 2.3. To assess robustness, a Noise-Artifact Experiment tests the model with white and EM noise, various artifacts, and different BSP electrode layouts. Additionally, real patient data from the EDGAR Database [16, 17] is used for validation.

Table 1 (E0) and Figure 4 present baseline reconstruction error results comparing our model with ZOT. ven if the RMSE value for our model is lower than that obtained with ZOT, the node-wise SCI boxplots show that our approach is more robust and less prone to outliers. ZOT show better values of SCI in most models, although it provides the worse as well, showing a great dispersion and presence of atypical values related to inverse SCI. DL model performs better in models 1 and 3, with the highest values of SCI of the set.

Noise robustness results are summarized in Table 1 for experiments E1-E4, where the DL model achieves an RMSE of 0.63 ± 0.015, slightly higher than ZOT's 0.52 ± 0.016 but with lower variability in DL's results. This indicates that although ZOT has a slightly better mean error, DL demonstrates less dispersion across experiments.

From E5 to E8 DL results are obtained to observe model behaviour when setting off patches of electrodes, as shown in Figure 1. These results do not include a comparison with ZOT, as this method do not take into account spatial disposition of electrodes. The results in these experiments again reflect the robustness of the model to electrode disconnection.

An alternative unfolding modality is tested to compare the impact of electrode order when creating the 2D matrix. Results in Table 1 for E9 against E0, with the same level of noise and all electrodes on show that there is a notable difference on the RMSE between the two settings, showing that the arrangement L-D-R-B-L (as explained in Figure 2) could lead to worse performance. This may be due to an inferior number of horizontal electrodes when using this order, or because the redundancy of frontal electrodes (F) rather than lateral electrodes (L) is beneficial for the model to learn meaningful correlations.

Finally, real AF patient predictions (Figure 3) show an average SCI of 0.3, suggesting lower reconstruction quality than with synthetic data.

4. Conclusions

Solving the ill-posed inverse problem in electrocardiography presents a complex challenge that AI could address in the near future. We propose a novel method for EGM reconstruction from BSPs of AF patients, which appears to be more robust than the gold-standard, although general performance still remains inferior. Although we are close

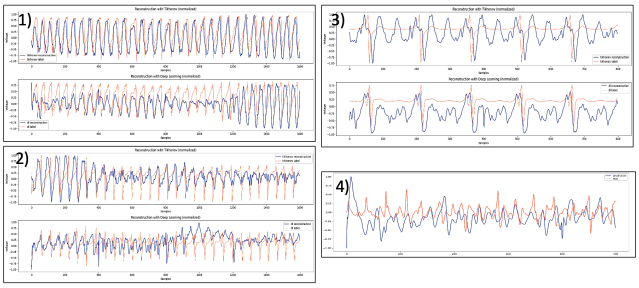

Figure 3. Plots from 1-3 are reconstructions obtained from synthetic models (AF Model 1, the one with better SCI, and AF Model 8, with the lowest SCI, as shown in Figure 4). Plot 4) is the econstruction of the EGM of a real AF patient.

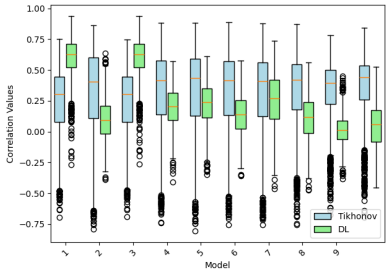

Figure 4. Boxplot representing the values of node-wise SCI in each AF model. Each box represents the values for all the nodes of test AF models.

Table 1. RMSE mean results for the test models with the different configurations of noise (E1-E4), electrode disconnection (E5-E8) and unfolding order (E0-E10)

Experiment ID	SNR EM Noise (dB)	SNR white noise (dB)	Electrodes off (patch)	Unfolding type	RMSE Test DL (Regression)	RMSE ZOT
E0	20	20	0	F-R-B-L-F	0.55	0.49
E1	1	5	0	F-R-B-L-F	0.65	0.55
E2	3	10	0	F-R-B-L-F	0.64	0.53
E3	5	20	0	F-R-B-L-F	0.64	0.51
E4	10	20	0	F-R-B-L-F	0.61	0.51
E5	20	20	Top right	F-R-B-L-F	0.59	-
E6	20	20	Top left	F-R-B-L-F	0.60	-
E7	20	20	Bottom right	F-R-B-L-F	0.61	-
E8	20	20	Bottom left	F-R-B-L-F	0.59	-
E9	20	20	0	L-F-R-B-L	0.61	-

to the solution of the problem, work should be done to balance the variance-bias tradeoff: bias must be reduced to improve the gold-standard in all AF signals. Next steps to boost performance include adding frequency information to the network input and train the models on real data, which contains less predictable AF patterns and artifact which represent a challenge to the machine.

Acknowledgments

This work has been partially supported by: Ministerio de Ciencia (PID2019-105032GB-I00, PID2022-136887NB-I00), Universidad Rey Juan Carlos (2023/ 00004/006-F918), Instituto de Salud Carlos III, and Ministerio de Ciencia, Innovación y Universidades (supported by FEDER Fondo Europeo de Desarrollo Regional PI17/01106 and RYC2018-024346B-750), Consejería de Ciencia, Universidades e Innovación of the Comunidad de Madrid through the program RIS3 (S-2020/L2-622), EIT Health (Activity code 19600, EIT Health is supported by EIT, a body of the European Union) and the European Union's Horizon 2020 under the Marie Skłodowska-Curie grant agreement No. 860974.

Address for correspondence:
Miriam Gutierrez Fernandez-Calvillo; Zorrotzaurreko Erribera, 2, 48014 Bilbao, Spain; mgutierrezf@vicomtech.org

References

[1] Tzeis S, et al. 2024 EHRA/Heart Rhythm Society/Asia Pacific Heart Rhythm Society/Latin American Heart Rhythm Society Expert Consensus Statement on Catheter and Surgical Ablation of Atrial Fibrillation. Europace 2024;.

[2] Griffin M, et al. Persistent atrial fibrillation ablation: Ongoing challenges defining the target population and substrate. Curr Treat Options Cardiovasc Med 2023;.

[3] Kistler PM, et al. Effect of catheter ablation using pulmonary vein isolation with vs without posterior left atrial wall isolation on atrial arrhythmia recurrence in patients with persistent atrial fibrillation: The capla randomized clinical trial. JAMA 2023;.

[4] Hernandez-Romero I, et al. Electrocardiographic imaging in the atria. Med Biol Eng Comput 2023;.

[5] Liu X, et al. Parallel spatial–temporal self-attention cnn-based motor imagery classification for bci. Front Neurosci 2020;.

[6] Tikhonov AN, et al. Solutions of Ill-posed Problems. 1977.

[7] Monaci S, et al. Non-invasive localization of post-infarct ventricular tachycardia exit sites to guide ablation planning: A computational deep learning platform utilizing the 12-lead electrocardiogram and intracardiac electrograms from implanted devices. Europace 2023;.

[8] Pilia N, et al. Non-invasive localization of the ventricular excitation origin without patient-specific geometries using deep learning. Artif Intell Med 2022;.

[9] Cámara-Vázquez M, et al. Non-invasive estimation of atrial fibrillation driver position with convolutional neural networks and body surface potentials. Front Physiol 2021;.

[10] Gutierrez-Fernández M, et al. Non-invasive atrial fibrillation driver localization using recurrent neural networks and body surface potentials. In 2022 CinC. 2022; .

[11] Rodrigo M, et al. Technical considerations on phase mapping for identification of atrial reentrant activity in direct- and inverse-computed electrograms. Circ Arrhythm Electrophysiol 2017;.

[12] Moody GB, et al. A noise stress test for arrhythmia detectors. In Comput. Cardiol. 1984; .

[13] Goodfellow, et al. Deep Learning. MIT Press, 2016.

[14] Bickel PJ, et al. Mathematical Statistics. 2015.

[15] Spearman C. The proof and measurement of association between two things. Am J Psychol 1904;.

[16] Aras K, et al. Experimental data and geometric analysis repository—edgar. J Electrocardiol 2015;.

[17] Pedrón-Torrecilla J, et al. Noninvasive estimation of epicardial dominant high-frequency regions during af. J Cardiovasc Electrophysiol 2016;.